Optical Materials: X 1 (2019) 100016

Contents lists available at ScienceDirect

Optical Materials: X

journal homepage: www.journals.elsevier.com/optical-materials-x

Invited Article

Optimized optical fiber poling configurations

Francesco De Lucia, Pier John Anthony Sazio*

Optoelectronics Research Centre, University of Southampton, Southampton, SO17 1BJ, UK

A B S T R A C T

The creation of an effective second order nonlinearity via the process of thermal poling in materials such as glasses, which naturally lack any second order susceptibility, has been known since the early 1990s. In this review, we present a historical overview via an introduction presenting early evidence of second order nonlinear effects in glass to explain the working principles of the thermal poling technique. An overview is then given to the transfer of the technique from bulk materials to optical fibers. Different configurations of poling are presented and compared, namely the conventional anode-cathode set-up, the development of the cathode-less process and most recently, the induction poling technique, which allows for poling fibers without any physical contact between the embedded electrodes and the high voltage supply. 2D-numerical models of the induction poling technique are later presented. An overview is also given of the different solutions for embedding electrodes inside the cladding holes of the fiber. Apart from solid electrodes, the more recent results have been presented about the adoption of liquid electrodes, both metallic and aqueous. For the first time silica optical fibers have been thermally poled using tap water as electrode. Both these two main results, namely induction poling and the liquid electrodes can allow to overcome some of the apparently intrinsic limits shown by the thermal poling technique so far, such as for example the length of the nonlinear devices and the complexity of the geometrical structure of microstructured optical fibres, both solid and PCF. Finally, we review the most recent outcomes and published applications of periodically poled silica fibers from our group, including high harmonic generation and phase sensitive amplification. All these promising results demonstrate that the way towards a full exploitation of the thermal poling technique for all-fiber nonlinear photonics is opening up many new vistas.

1. Introduction

Although the concept of “total internal reflection” (TIR) was known since 1854 [1] and the first glass optical fibers were realized in the 1920s [2,3], it was only in the 1970s that optical fibers started to become what they had promised to be in the previous fifty years, namely reliable waveguides to transmit information, thanks mainly to the work of Kapron et al. [4], who realized for the first time single mode waveguides characterized by reasonably low intrinsic transmission losses (7 dB/km). Since then the performances of optical fibers, in terms of transmission losses, have improved dramatically, allowing them to transform the telecommunication world. Nowadays it is possible to dope optical fibers with erbium to obtain optical amplifiers, or with ytterbium or neodymium to get fiber lasers, or to integrate Bragg gratings mirrors and filters into them. Nevertheless, their enormous global deployment is mainly for passive photon-based data transport rather than as a platform for nonlinear photonic devices (such as for example frequency converted laser sources, beam modulators and switches, optical sensors, etc.). The main reason of this limited use is the lack of intrinsic second order nonlinear properties in centrosymmetric materials, such as silicate glasses, which are exploited to fabricate most of optical fibers. This means that conventional step index silica optical fibers could not be used to generate second order related nonlinear parametric effects [5]. However there exists a method, called thermal poling, developed in 1991 by Myers et al. [6], to generate effective second order susceptibility $\chi^{(2)}_{eff}$ in glasses. The method allows a permanent second order nonlinearity to be induced in a medium which is poled via the application of a static electric field, while it is heated up to a temperature whereby alkali impurity ions inside the material have a non-negligible diffusion and drift mobility. The thermal poling technique was initially adopted to create a quadratic nonlinearity inside bulk glasses but afterwards the idea of using it with optical fibers started to gain interest. The main motivation behind the idea of exploiting the quadratic nonlinearity inside an optical fiber comes from the purpose of overcoming some of the issues affecting the conventional approach for realizing nonlinear optical devices, based substantially on the standard scheme which considers the interaction between intense light waves and nonlinear crystals (such as for example *lithium triborate* (LBO), *beta-barium borate* (BBO) or *lithium niobate* ($LiNbO_3$)). Some of the drawbacks are the thermal instabilities of the nonlinear crystals when illuminated by very powerful laser radiation [7,8], the relatively short interaction lengths between light waves involved in the nonlinear process, high costs and low damage thresholds of the crystals, coupling losses due to the presence of air/nonlinear crystal interfaces as well as the onerous requirement for continuous optical alignment necessary in free-space optical setups. Most of the reported drawbacks could be

* Corresponding author.
E-mail address: pjas@soton.ac.uk (P.J. Anthony Sazio).

https://doi.org/10.1016/j.omx.2019.100016
Received 23 April 2019; Accepted 9 May 2019
Available online 28 May 2019

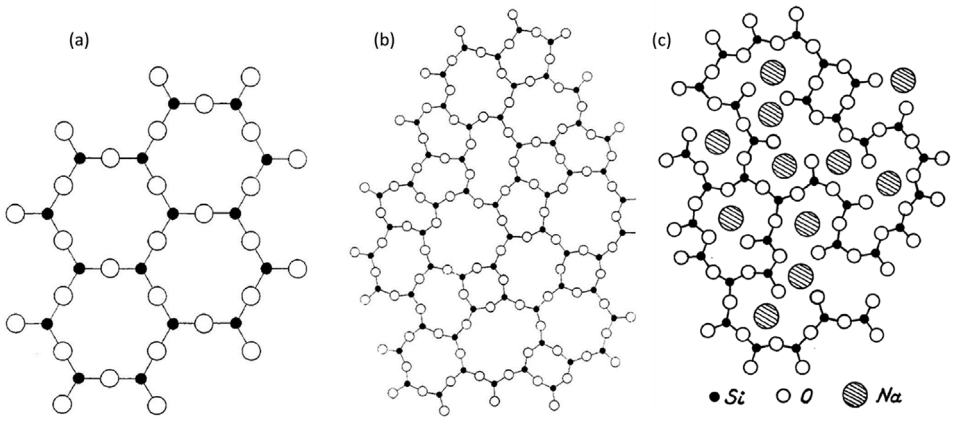

Fig. 1. Schematics of the arrangement in two dimensions of (a) a crystal of composition A_2O_3 and (b) the glass network of the same compound. The letter "A" stands for a whatever atom of a silicate group bound to the three oxygen atoms in the 2D crystal [10]. (c) Two dimensional schematic diagram of the soda-silica glass structure. It can be seen that there are some oxygen atoms bonded to two silicons whereas some others to just one silicon [11]. The sodium ions are located into the holes of the $Si-O$ network, and represent impurities into the glass structure.

almost completely overcome by realizing an all-fiber nonlinear device, where the light waves could not only be delivered with very low losses but also generate second order nonlinear processes.

2. Structure of silicate glasses

A glass is defined by the American Society for Testing Materials (ASTM) [9] as an "inorganic product of fusion which has been cooled to a rigid condition without crystallization", so it is considered a branch of the group of amorphous solids whose atomic structure lacks the so-called "long range regularity" typical of a crystalline material, as explained in Fig. 1.

If we consider the most common kind of glass, called vitreous silica (or fused quartz), we see that the basic molecule which defines its composition is SiO_2 (silicon dioxide). In this type of glass each silicon is bonded tetrahedrally to four oxygens at a distance of $Si-O = 0.162$ nm while each oxygen is bonded to two silicons [12]. Different varieties of silica glass can be obtained by melting SiO_2 with other raw materials. If for example some Na_2CO_3 (soda, or sodium carbonate) is added to the initial molten mixture, it is possible to create the so-called soda-silica glass. In this case, because of the oxygen introduced by the soda, each silicon is still bonded to four oxygens, while each oxygen cannot be bonded anymore to two silicon atoms, in such a way that there are two types of oxygen bonds, those with two silicon atoms and those with just one silicon, also defined as non-bridging oxygen (NBO) centres [13]. In other words, there are holes in the silicon-oxygen network, and it is in these holes that the sodium ions Na^+ are situated randomly, surrounded by approximately six oxygens as immediate neighbours [11]. In Fig. 1(c) the two dimensional schematic diagram of the soda-silica glass is shown. Any phenomenon of electrolytic conductivity produced in glasses like soda-silica can be seen as the stepwise series of displacements of the Na^+ ions between each of the holes in the $Si-O$ network. A glass can be made of many of these inclusions, such as for example Ca^{+2}, K^+, Pb^{+2}, Li^+, etc [10].

3. Early evidences of second order nonlinearities in silica fibers

An amorphous dielectric medium can be considered macroscopically isotropic and centrosymmetric and then invariant by parity inversion, the operation which transforms a vector in another one characterized by the same spatial coordinates in absolute value but with the sign inverted [9]. In centrosymmetric materials the relationship between the polarization and the electric field of the light wave interacting with the medium possesses an odd symmetry, which means that the polarization vector lacks any term of even power of the electric field [14]. Therefore, a glass, which is an amorphous medium, should lack the second order nonlinear susceptibility $\chi^{(2)}$, because of the parity invariance [5]. So, in silica fibers $\chi^{(2)}$ is nominally zero and the nonlinear effects related to the second order susceptibility are negligible. Nevertheless, in the 1980s there were experimental observations of some nonlinear effects in optical fibers. In particular, in the period 1980–1982 the early observations of phase-matched SFG by using waveguide modes of optical fibers were reported. A Q-switched and mode-locked Nd:YAG laser at 1064 nm wavelength was used as pump source and the sum-frequency light was generated from the pump and the Stokes lines due to inelastic (Raman) scattering in optical fibers [15–17]. The first ever reported observation of SHG in optical fibers was by Gabriagues et al. [18] while a few years later Osterberg et al. realized the first detailed study related to the SHG in a silica fiber pumped with 100–130-psec-long pulses and peak powers of 70 kW produced by a mode-locked and Q-switched Nd:YAG laser. After a certain period of illumination, weak second-harmonic radiation was observed at the output end of the fiber and, after a certain time of "preparation", the intensity of the green light increased [19,20]. Later on it was observed that the "preparation" time could be reduced (from hours to minutes) if, together with the pump pulses, the fiber was also illuminated by light pulses with the same wavelength as the second harmonic wavelength [21]. Two models were proposed to explain this SHG in optical fibers. According to Farries et al. [22] a weak non-phase-matched SHG occurs at high pump intensities due to a nonlinear electric quadrupole susceptibility and initiates the self-writing of an axially periodic pattern of colour centres (created at spatial locations where the green light intensity is highest, i.e. where the pump and second-harmonic signal are in phase) which would lead to the growth of a $\chi^{(2)}$ grating [23]. The second model was proposed by Stolen et al. who assume a photoinduced effect which forms the dipole-allowed second order susceptibility. Basically, the pump and the external (or even the internal) seeding light (of frequency corresponding to the second harmonic of the pump) mix by means of a third order nonlinear optical rectification process to create a DC polarization at the phase-matching periodicity which orients the defects. The oriented defects can produce a direct dipole-allowed nonlinear susceptibility $\chi^{(2)}$, which has the proper periodicity for phase-matched SHG [21]. Therefore, the fiber self-organizes for phase-matching and the permanently written periodic nonlinearity created into the fiber produces an efficient SHG in the fiber. Limitations of the photoinduced second order nonlinear effects generated in optical fibers, such as for example the length of the self-written phase-matched gratings, which is limited by the chromatic dispersion of the medium and the phase modulation as well as the relatively low estimated SH efficiency [24] and the dependence of the SH efficiency on the dopants/defects in the glass [25], made them a relatively unattractive proposition as a frequency conversion device. Nevertheless, significant efforts were expended to make these nonlinear phenomena in optical fibers much more efficient, and the dream of replacing expensive nonlinear crystals with cheap all-fiber nonlinear devices was not completely abandoned. Given the assumption that the origin the self-written grating was the DC polarization generated by a third order nonlinear optical rectification process, the idea of exploiting

DC electric fields applied externally to the fiber started to gain traction amongst researchers in optical fibers. Eventually, Kashyap demonstrated the possibility to generate a phase-matched electric-field-induced second harmonic (EFISH) in single-mode Germania-doped silica fibers [26]. By using a rotatable interdigitated electrode structure, it was possible to apply a spatially varying electric field across the core, which is periodic along the propagation direction of the fiber. As a result, the spatial static field induces a periodic effective second order nonlinearity $\chi^{(2)} \propto \chi^{(3)} \cdot E$, where E is the electric field applied across the core and $\chi^{(3)}$ is the third order nonlinear susceptibility of the silica glass that the optical fiber is made of. The rotation of the electrode allows for the control over the periodicity of the applied electric field which compensates the wave-vector mismatch between the pump and the second harmonic propagating along the fiber.

4. Thermal poling

Although the work of Kashyap [26] demonstrated the possibility of producing efficient SHG in optical fibers by means of an external periodic electric field which induces third order nonlinear optical rectification, the SHG was still a temporary effect, in the sense that as soon as the externally applied electric field was removed, the second harmonic generation process would stop. However, in 1991 Myers et al. demonstrated the possibility of inducing a large permanent effective second order nonlinear susceptibility ($\approx$1 p.m./V) in centrosymmetric materials such as bulk silica glass [6]. The method is called thermal poling and consists in the application of a high potential (3–5 kV) through a bulk piece (thickness of 1.6 mm) of fused silica heated up at a temperature in the range 250–325 °C for a time between 15 and 120 min. The heating process is followed by a cooling process during which the difference of potential is still maintained across the sample. It was demonstrated that the nonlinearity is induced permanently only in the first few microns of the sample near the surface where the anodic potential is applied. The SH signal was measured by illuminating the bulk sample with 10 ns and 10 MW/cm^2 pulses generated by a Q-switched Nd:YAG laser with a repetition rate of 10 Hz and collecting the SHG signals by means of a photomultiplier tube (signal to noise ratio of 500:1). The value of $\chi^{(2)}$ induced was evaluated by comparison of the SHG signals with those generated by two reference samples, namely a quartz crystal (the crystalline form of SiO_2) and a crystal of $LiNbO_3$, whose values of $\chi^{(2)}$ are well known. They found that the $\chi^{(2)}_{33}$ value for fused silica is 20% of the typical value of the $\chi^{(2)}_{22}$ measured for $LiNbO_3$. An important experimental observation realized in this first poling attempt comes from the comparison of the different values of second order nonlinearities measured for different types of silica glasses tested (Optosil™, Homosil™, Infrasil™ and Suprasil™), in particular the fact that the values were all similar apart from the one induced in Suprasil™ (characterized by a concentration of "impurities" much smaller than the others), which is one order of magnitude smaller. The fact that the induced effective $\chi^{(2)}$ is smaller in a glass with a lower concentration of impurities already suggests that they play an important role in the thermal poling process.

4.1. Theoretical explanation of the thermal poling process

In 1994 a first attempt of explaining theoretically the dynamics of the thermal poling process was realized by Mukherjee et al. who proposed a model based on simple ionic charge transport together with bonds reorientation [27]. It assumes that, because of the application of the external electric field, the impurity charges present in the glass sample re-organize themselves in order to generate locally static electric fields which in turn orient the bonds (related to impurities or $Si-O$ bonds). The induced $\chi^{(2)}$ is expressed by:

$$\chi^{(2)} \approx \chi^{(3)} E_{DC} + \frac{np\beta}{5k_B T} E_{DC} \quad (1)$$

where the first term of the right-hand side represents a third order nonlinear optical rectification process with $\chi^{(3)}$ being the third order nonlinear susceptibility of the material that the fiber is made from and E_{DC} represents the static electric field created in the poled sample by means of a charge transport process. The second term of the right-hand side describes the electric-field-induced orientation of the molecular second order hyperpolarizability, with k_B the Boltzmann constant, T the absolute temperature of the sample, p the permanent dipole moment associated with the bond, N the number of dipoles involved in the process and a uniaxial molecular system assumed for the sake of simplicity. The work of Mukherjee et al. introduced for the first time the concept of depletion region formation, that is the creation of a space-charge region, located near the anodic electrode, which is depleted of ionic charge impurities. This region consists of the *NBO* centres, already introduced in section 1, which have lost the ionic charges initially electrostatically bonded to them, because of the application of the external electric field at high temperature (and subsequent relatively high mobility of the ions).

In 1998 Alley et al. studied the dynamics of formation of the space-charge region in thermally poled fused bulk silica [28]. The most relevant experimental observation were multiple time scales for SH signal formation, which requires the presence of carriers characterized by different mobilities. Alley et al. postulate that the space-charge region formation is heavily affected by the injection of hydrogenated species (such as H^+ or H_3O^+). If these hydrogenated species, characterized by a much smaller mobility than the impurity charges ($\mu_{H^+} \approx 10^{-4}\mu_{Na^+}$) are present at the fused silica surface, produced by high field ionization or from field-assisted evolution of $O-H$ bonds into H_3O^+ [29,30], they can be injected into the glass matrix and contribute to the space charge formation via a field assisted ion exchange process, which consists of a slow replacement of the impurity charges removed from the *NBO* centres with the hydrogenated ions injected. An important observation by Yamamoto et al. is that glass surfaces are much more hydrated than the bulk, confirming in this way the possibility of an enormous reservoir of hydrogenated species ready to be injected into the glass matrix at high temperature.

In 2005 Kudlinski et al. published a more complete description of space-charge region formation and induced second order nonlinearity in bulk silica glasses [31]. The samples used in this work were disks of fused silica (Infrasil™) of different thickness, sandwiched between two *Si* electrodes, heated at 250 °C, and poled at 4 kV for different temporal durations. The value of $\chi^{(2)}$ induced in the poled samples was estimated by means of the "layer peeling" method presented in a previous work of Kudlinski et al. [32]. This method allows for measuring the $\chi^{(2)}$ at different depths inside the glass sample under investigation. The description of the dynamics of the space-charge region formation assumes that, because of the application of the voltage (V_{app}) through the whole sample of length l, an electric field is established equal to (V_{app}/l) and, because $\mu_{Na^+} \gg \mu_{H^+}$, initially a depletion layer beneath the anodic surface of the glass is created due to the sodium ion migration toward the cathode. The induced electric field at the surface increases and screens the applied electric field in the region of the sample located outside the depletion region. The maximum value of E_{DC} ($\approx 10^9$ V/m) is reached when the space-charge region is fully established. At this time the concentration of the injected carriers per second increases quickly reaching a value of $7.5 \times 10^{22} m^{-3} s^{-1}$ (according to the equation defining the charge injection into the glass of the hydrogenated species, which establishes that the concentration of those species at the anodic surface is linearly proportional to the value of the electric field at the same surface). At the same time, the drift velocity of these injected hydrogenated species $v_{H^+} = \mu_{H^+} E_{DC}$ becomes comparable to the velocity of the sodium ions, which are located outside the depletion region, where the applied electric field is actually reduced because it is screened by the presence of the space charge. For poling times longer than few minutes, these injected ions move deeper and deeper into the glass replacing little by little the previously removed sodium ions,

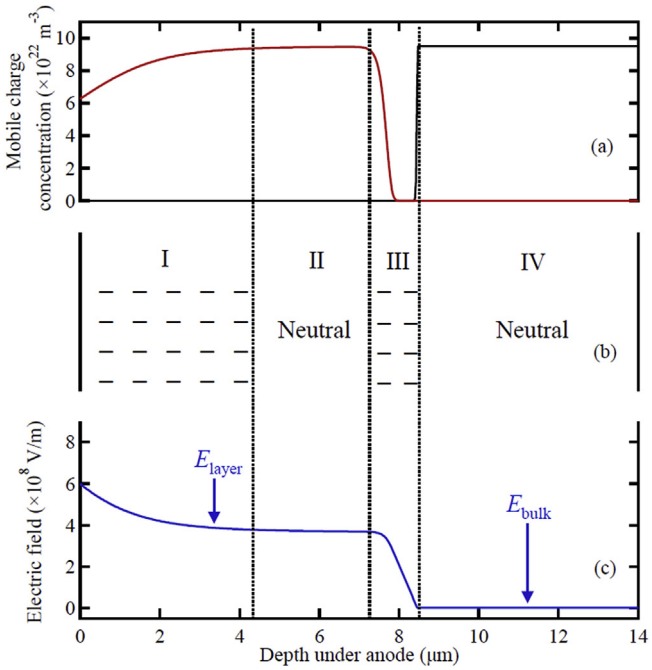

Fig. 2. Theoretical results related to a 200 μm thick sample of fused silica (Infrasil™) poled for 100 min. (a) Representation of the mobile charge concentration (the black line represents the sodium density while the red one the injected carrier density); (b) schematic of the charge distribution; (c) electric field distribution [31]. (For interpretation of the references to colour in this figure legend, the reader is referred to the Web version of this article.)

neutralizing in this way the *NBO* centres. In Fig. 2 the evolution of the space-charge region after a poling time of 100 min is reported as expected by the model of Kudlinski et al. [31].

4.2. From poling of bulk glasses to silica optical fibers

The first attempt of poling a silica fiber was realized by Kazansky et al. in 1994 [33], when a D-shaped fused silica Germania-doped step-index fiber was poled using the setup reported in Fig. 3(a).

After some development where the same poling configuration was used, in 1995 a twin-hole step-index silica fiber was poled for the first time by applying a difference of potential between two electrodes inserted respectively into two holes running along the fiber [34]. Fig. 3(b) reports a cross-section of this kind of fiber, which became the new standard geometry for thermal poling of optical fibers [35–39].

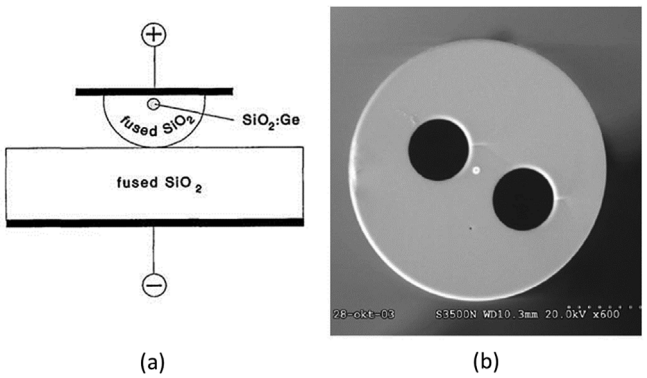

Fig. 3. (a) Schematic of a D-shaped optical fiber arranged for thermal poling. The side-polished fiber is placed on top of a silica substrate and the whole setup is sandwiched between two electrodes through which the voltage is applied. The setup is placed inside an oven [33]. (b) SEM image of a twin-hole silica fiber for thermal poling via internal electrodes [39].

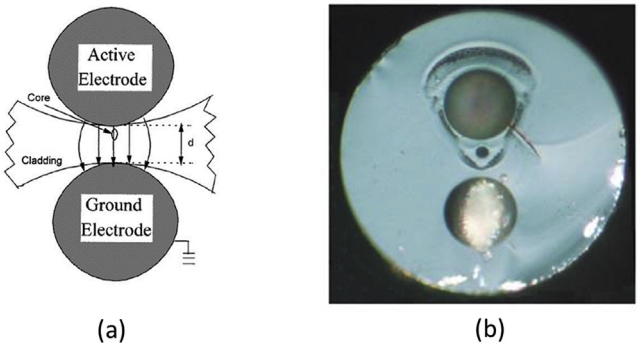

Fig. 4. (a) Schematic of the electrical configuration anode-cathode for thermal poling of silica fibers [36]. (b) Cross-section of a twin-hole silica fiber poled via the anode-cathode configuration and etched in HF for 1 min [40]. The ring visible around the hole where the anode is located represents the space-charge region whose mechanism of formation has been described in section 3.1 [39]. As expected, according to the electromigration mechanism of the impurity charges, the space-charge region develops only around the anodic surface.

4.2.1. Conventional poling

The conventional anode-cathode configuration for thermal poling of silica fibers, shown in Fig. 4(a), produces a space-charge region which develops only around the hole where the anodic electrode is inserted. The space-charge region can be visualized by means of a decorative etching process of the cleaved facet of the poled fiber in HF (diluted at 50% in DI water) for 1 min and is reported in Fig. 4(b). The anode-cathode configuration is however affected heavily by the limit of the small distance (≈10–20 μm) between the two holes where the electrodes are embedded, which increases significantly the risk of breakdown through the silica glass due to the application of high voltages.

4.2.2. Cathode-less poling

In 2009 Margulis et al. demonstrated that it is possible to create a depletion region around both the electrodes inserted in the cladding holes of a twin-hole silica fiber by connecting them to the same anodic potential, without contacting any electrode to the cathode of the voltage supply [41].

Fig. 5(a) shows the cross-section of an example of twin-hole silica fiber poled in this cathode-less configuration. This new poling configuration allows for reducing the risk of electrical breakdown through the fiber during the poling process. In the work of Margulis et al. it was also experimentally observed that the effective second order nonlinearity created by means of this method is larger than the one created by means of conventional anode-cathode configuration and furthermore demonstrated that the new method of poling (or "charging", according to their definition) is more stable than the conventional one in terms of in terms of "degradation time" of the $\chi^{(2)}$ at 250 °C. The theoretical explanation of the depletion region formation in the "cathode-less" configuration requires the introduction of a mechanism called "avalanche-like positive feedback". Considering the two-dimensional plot of the equipotential surfaces in a fiber before any charge transport starts (see Fig. 5(b)), and assuming that both the electrodes are at the same positive potential (+5 kV) and the external surface of the fiber is grounded by means of the negative charge supplied by the air, Margulis et al. highlight that the potential at the fiber core is approximately 500 V lower than the potential at the two electrodes. Therefore, the ionic charge transport starts (at high temperature) because of this small potential difference. A depletion region begins to be created around both the anodes, even if it is not circular at the beginning. This non-circularity of the depletion region modifies the uniform distribution of ions at the beginning of the process. Because of the positive charge migration from the electrodes, there is an increase of the resistivity of the glass, which produces a drop of the potential at the core of the fiber. This situation creates even more charge displacement and increases the

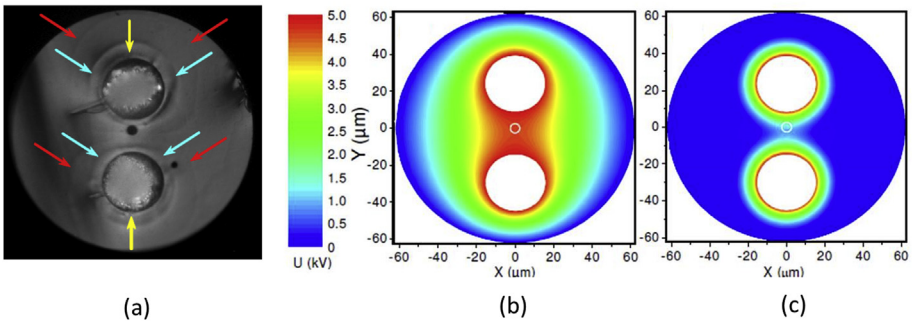

Fig. 5. (a) Cross-section of a twin-hole silica fiber poled using the double-anode configuration and etched in HF [42]. (b) and (c) represent the equipotential maps of a fiber subjected to an electrical potential of 5 kV applied to both the internal electrodes, assuming electrically grounded the outer surface of the fiber. Specifically (b) represents the initial situation, where there is a small drop of potential between each electrode surface and the fiber's core, due to the non-zero resistivity of the glass. (c) Shows the situation after a certain time, when a depletion region has been already created and the drop of potential through the core has grown because of the increase of the resistivity of the core region, due to its depletion from impurity charges [41].

potential difference between the electrodes and the centre of the fiber. This process of "avalanche-like positive feedback" finally results in a complete depletion, such as in conventional poling processes.

4.2.3. Induction poling

The cathode-less method for poling optical fibers, invented by Margulis et al. in 2009, represented the state of art for thermal poling until 2014. Although this novel method allowed for simplifying the poling technique in terms of embedded electrodes configuration, it still did not solve some of the issues which prevented thermal poling from being a reliable and facile technological platform for realizing all-fiber nonlinear photonic devices. One of the principal issues is for example represented by the length L (which is an important parameter because the efficiency (η) of the second order nonlinear effects depends on it, for example in the second harmonic generation η scales quadratically with L) of the poled fiber, limited by the manual insertion of very small diameter ($\phi \approx 20 - 25\ \mu m$) metallic wires used as electrodes inside the cladding holes of the fiber. The manual insertion, apart from being limited by human capability to just a few centimetres of length and also being a very time consuming and tedious process, is also characterized by the inhomogeneity of the space-charge region depth along the fiber length, due to the fact that the wires inserted do not fill completely the holes where they are inserted. An alternative approach to the issues presented by the manual insertion of the electrodes was proposed by Knape et al. in 2007 [43]. The electrodes were embedded by pumping into the two cladding holes eutectic alloys such as *BiSn* (melting temperature of 138 °C) or AuSn (melting temperature of 280 °C) in their molten state. The electrical connection to both the embedded electrodes is realized by side polishing the fiber against two points of the two channels and inserting the wire inside each hole while the alloy (re-solidified at room temperature) is locally re-melted to ensure a robustly bonded electrical connection (see Fig. 6). Although this approach allows an increase in length of the poled fiber to reach potentially a few metres, it presents some practical issues. For example, the requirement for side polishing results in a low device yield because the probability of breaking fibers during the various phases of the poling process is very high. The other relevant issue of this approach is the need of removing the eutectic alloy from the two cladding holes of the fiber. The presence of the metal greatly increases the transmission losses of the poled fiber because of the overlap between the traveling mode and the metal present inside the channels. For some applications, such as for example frequency doubling, reducing the losses is a primary target, so the removal of the metal is critical. The difficulty of removing the electrodes is due to the fact that the whole fiber needs to be heated up to a temperature higher than eutectic melting temperature and then pressurized in order to let the metal escape from the channels.

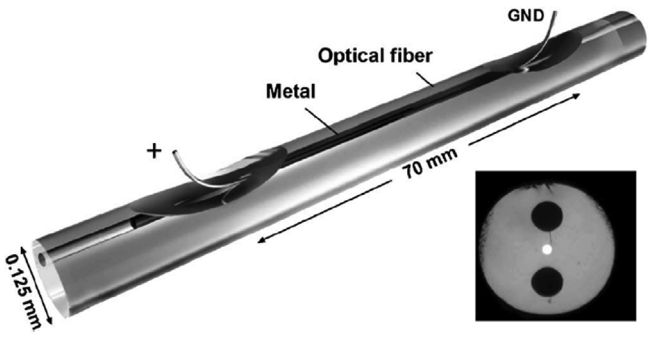

Fig. 6. Schematic picture showing a twin-hole fiber equipped with two molten metal electrodes. The two channels are side polished to allow to access the electrodes with the wire used for the connection to the anodic and ground potential respectively [43].

4.2.3.1. Experimental setup. Besides the issue of the removal of the metallic electrodes there is another problem not addressed by the method of Knape, represented by the need of a physical contact between the embedded electrodes and the high voltage power supply. In 2014 De Lucia et al. invented a new method for poling silica fibers, defined as "electrostatic induction" poling [44]. A first fiber (the inductor), of a relatively short length, equipped with internal solid electrodes and a second one (the sample to be poled), much longer than the first one and equipped with embedded electrodes as well, are placed on top of a microscope slide in turn located on top of a heater. The two fibers are kept adjacent over a distance of a few centimetres and while the electrodes embedded in the inductor are both connected to the chosen anodic potential, the two electrodes embedded inside the sample to be poled by induction are left floating. The backside of the microscope slide is coated with Gold and represents the ground plane of the system. The setup for induction poling is shown in Fig. 7.

The first test of the success of the induction poling method was conventional decorative etching in *HF*, whose result is reported in Fig. 7(b). The cross section reported in the figure confirms the formation of a depletion region around both the holes containing the embedded floating electrodes. The etching procedure has been repeated all along the 40 cm of length of the sample to be poled, showing always the formation of a depletion region, confirming that the technique allows poling without any physical contact (between the high voltage power supply and the embedded electrodes) to a fiber significantly longer than the inductor. The creation of an effective $\chi^{(2)}$ by *induction poling* has been also proven via the measurement of a second harmonic signal after phase-matching the pump at 1550 nm and the SH light at 775 nm via periodic UV erasure of the nonlinearity.

In Fig. 8(a) the setup for the UV erasure and the subsequent characterization of the second harmonic signal is reported while in Fig. 8(b) the two peaks of the SHG signal measured for the two different periods of UV erasure realized on two samples poled in the same experimental conditions are shown. The dependence of the wavelength doubled from the period of the erasure confirms that the signal measured is due to a SH signal created by a second order nonlinear process via *induction poling*.

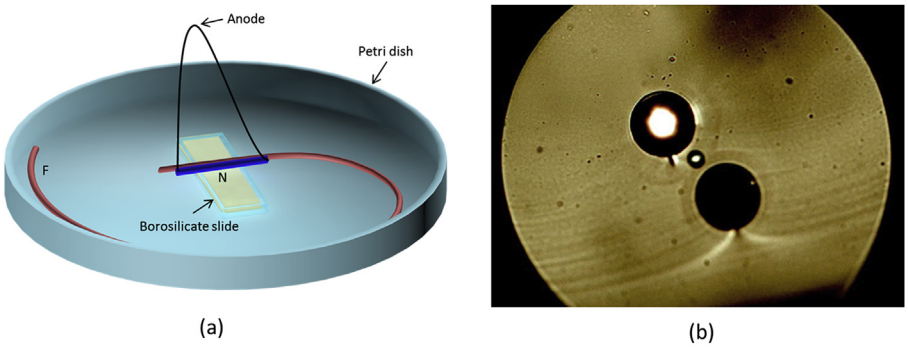

Fig. 7. (a) Schematic of the experimental setup for induction poling of optical fibers. The inductor is coloured blue and equipped with two electrodes (tungsten wires) connected to the same anodic potential. This fiber serves as a dielectric barrier to prevent unwanted electrical breakdown in air. The red fiber (equipped with two embedded floating electrodes) is the sample to be poled. Both inductor and sample are adhered to a borosilicate slide and held in close proximity. The slide has a thin metallic layer evaporated onto its rear surface held at ground potential. The Petri dish is kept at an almost constant temperature of ≈300 °C for the whole duration of the poling process. (b) Twin 19-μm holes in silica fiber with Germania-doped core. The depletion regions generated via electrostatic induction poling are visible after etching. A gallium electrode has been selectively purged, highlighting the versatility of the technique [44]. (For interpretation of the references to colour in this figure legend, the reader is referred to the Web version of this article.)

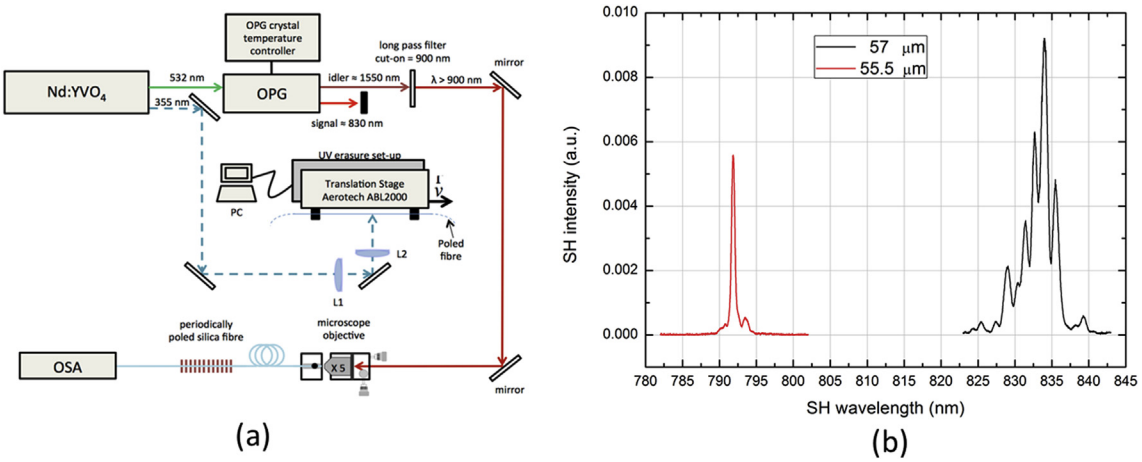

Fig. 8. (a) Experimental setup for the inscription of the quasi-phase matching (QPM) grating in the induction-poled fiber by 355 nm erasure. L1 and L2 are cylindrical lenses of focal lengths *f* 500 mm and 85 mm, respectively, used to produce a spot size on the fiber of 10 μm × 100 μm. The optical setup used for the SHG nonlinear characterization of the periodically poled fiber is also shown [44]; (b) SHG spectra of induction poled samples with different QPM grating periods written via UV erasure.

4.2.3.2. 2D numerical model. After the experimental proof of the induction poling method, in 2016 De Lucia et al. published the 2D numerical model of the dynamic process of formation of a depletion region in a twin-hole fiber poled by electrostatic induction [45]. This builds on the numerical model produced by Camara et al. in 2014 [42], but presents some critical modifications. The first difference is in the assumption that the outer surface of the fiber is always at ground potential. While this assumption is reasonable when considering the experimental setup described in the work of Margulis et al. [41], an external field applied by an inductor to floating electrodes inside fibers would, by definition, be fully shielded by this grounded surface, thus completely inhibiting the induction poling process. Furthermore, the model of Camara et al. concludes that field-dependent H_3O^+ ion injection, which only becomes significant for longer poling times, does not differ significantly from constant rate injection conditions, given that the electric field at the anode-glass boundary reaches a value of $\approx 10^9$ V/m over a short time period and then remains constant. However, in the induction poling geometry, the variable floating potentials inherent in this process require a field-dependent charge injection scheme. Finally, it is also necessary to modify the field dependency to take into account ion recombination at the cladding-air interface. We show that mapping the salient features of the induction poling experimental geometry allows us to draw a more appropriate set of boundary conditions, and the modified 2D model can then be used to describe the dynamics of the second-order nonlinearity created inside the fiber when it is both close to and far away from the external inductor. The model for induction poling of long samples can be implemented simply dividing the model into two sub-models, one conceived to describe the dynamics of the electromigration process in the part of the setup where the two fibers (inductor and sample) are close each other (called *near model*), and one for the part of the setup where the sample is far from the inductor (called *far model*). Fig. 7(a) distinguishes clearly the two sections of the setup described by the two different sub-models. The main difference between these consists in the fact that in the first case the sample is immersed in the electric field lines generated by the externally applied electric field while in the second case it is not. The reliability of this "double" model assumes electrical continuity of the electrodes embedded into the sample to be poled. The working principle of the electrostatic induction poling of long samples is based on the idea that, when the two floating electrodes, embedded into the sample, are immersed in the external electric field (supplied by the inductor in the region where the two fibers are in proximity), they pick up the electric field, become electrically charged because of an electrostatic induction process and so reach a certain electric potential. Furthermore, due to the fact that during induction poling, there is very little, if any, current flow through the fiber; therefore, as there is virtually no voltage drop due to metallic series resistance, the internal floating electrodes will present a well-characterized equipotential surface throughout the entire sample. This means that any electric potential picked up by the floating electrodes close to the inductor will be effectively transferred to any remote location throughout the fiber. The numerical model assumes that the inductor is made of a glass totally lacking any impurity charge inside, while the sample is assumed to be a fused silica twin-hole with an initial

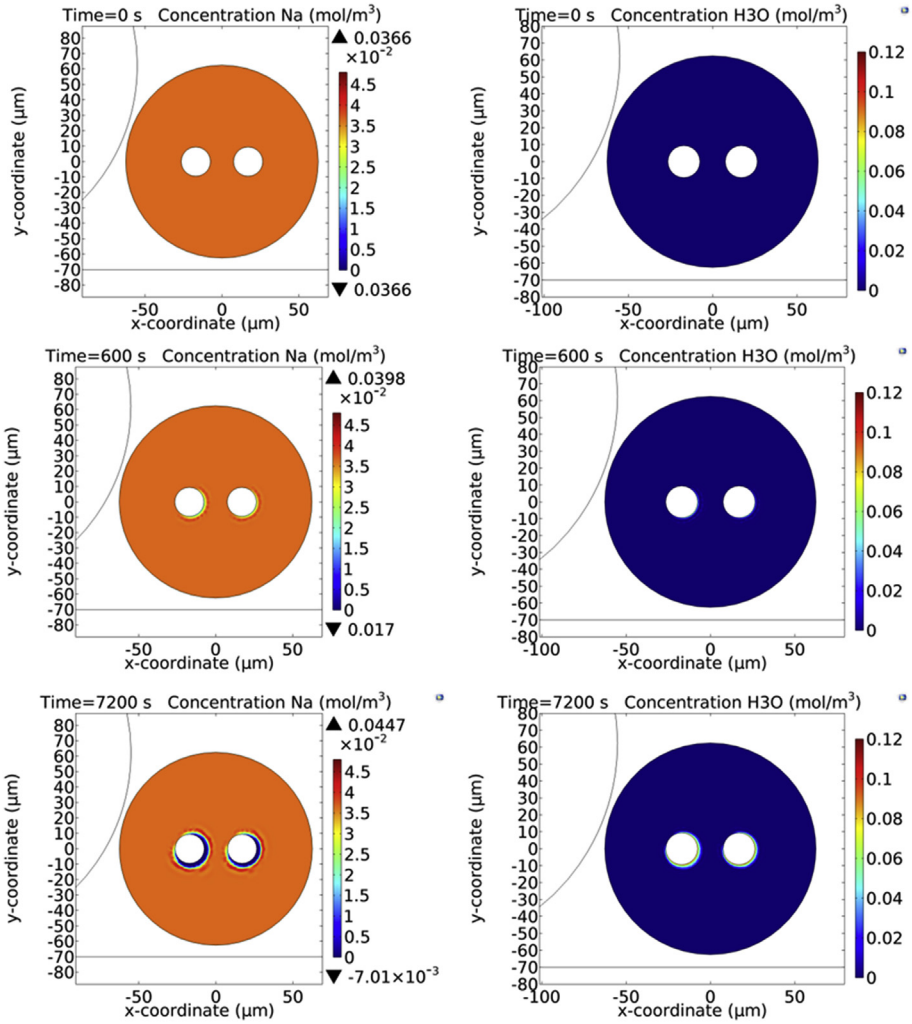

Fig. 9. Temporal evolution of the mobile positive ions obtained via the *near model* for induction poling. Only the electromigration inside the sample to be poled is considered, while the mobile ions of the inductor are assumed absent. The external surface of both the fibers is not grounded while the ground plane is located at 1 mm distance below the two fibers. The initial concentration of the impurity charges (Na^+) is arbitrarily assumed to be 1 ppm. The temperature of the sample in the simulation is assumed to be 300 °C while the injection of the hydrogenated species H_3O^+ is assumed to be inexhaustible and capable of neutralizing the *NBO* centres depleted of impurity positive ions due to the application of an external electric field. The voltage applied to both the electrodes embedded into the inductor corresponds to +5 kV.

concentration of 1 ppm of Na^+. It is also assumed that in the sample there is up to 1 ppm of H_3O^+ ions injectable at the cladding holes, with none present within the fiber at t = 0 s. To achieve initial charge neutrality, negatively charged, non-bridging oxygen sites (*NBO*) with extremely low mobility are uniformly distributed inside the sample with a concentration of 1 ppm at t = 0 s. The cladding holes are also assumed to be entirely filled with metal electrodes and present an equipotential. Furthermore, H_3O^+ ions can be injected through the electrode-cladding surface when located at electric potentials higher than the surrounding cladding. An adjustable parameter σ_2 (whose value is chosen to be the same as the well-established thermal poling model reported in Ref. [31]) is used to describe the charge injection into the sample. It is also necessary to consider the special case where the electric field is less than zero. In this case, H_3O^+ ions in the nearby cladding (either previously injected or diffused from other parts of the fiber) will have a negative injection rate, thus implying an out flow of H_3O^+ ions. However, if there are not any H_3O^+ ions (i.e., c (H_3O^+) = 0) at the electrode-cladding boundary, the injection rate will be zero, even with an electric field less than zero. Therefore, the variation of the injected H_3O^+ density per unit of time at the electrode-cladding surface can be written as:

$$\left(\frac{\partial c_2}{\partial t}\right)_{surface} = \sigma_2 E, \quad E \geq 0 \; or \; E < 0 \; and \; c_2 > 0 \tag{2}$$

$$\left(\frac{\partial c_2}{\partial t}\right)_{surface} = 0, \quad otherwise \tag{3}$$

where c_2 indicates the concentration of the H_3O^+ species and σ_2 the constant chosen. In the *near model* the two fibers are co-located, immediately adjacent each other, on top of a borosilicate microscope slide of 1 mm of thickness, which can be equipped on its back face with a metallic coating which is grounded. The *far model*, instead, consists in the model of Camara (modified according to the considerations reported at the beginning of this section) where the values of the electric potential applied to the two embedded floating electrodes are not anymore considered constant, but are exactly the variable (in time) values of electrostatic potential calculated by means of the *near model*. Furthermore, it will be assumed that the sample, located on top of the microscope slide, will be always in a condition of an "absent" ground plane, because actually the only ground reference is a poorly-defined ground plane, given by the heater coil, which cannot be modeled. Fig. 9 shows the temporal evolution of the concentrations of both the "fast" and "slow" carriers (respectively Na^+ and H_3O^+) calculated at three different times of the induction poling process in the *Near model*, while in Fig. 10 the concentrations are shown for the *Far model*. It is worth noting that, even if the electric equipotential surfaces of the floating electrodes near and far from the inductor evolve in time in the same way, the two depletion regions develop differently in the two different locations. This is due to the presence of the external electric field of the inductor, which modifies the total electric field distribution around each electrode, compared to the situation far from the inductor. A different distribution of the electric field in the space around the electrodes will determine a different evolution of the depletion region in these positions.

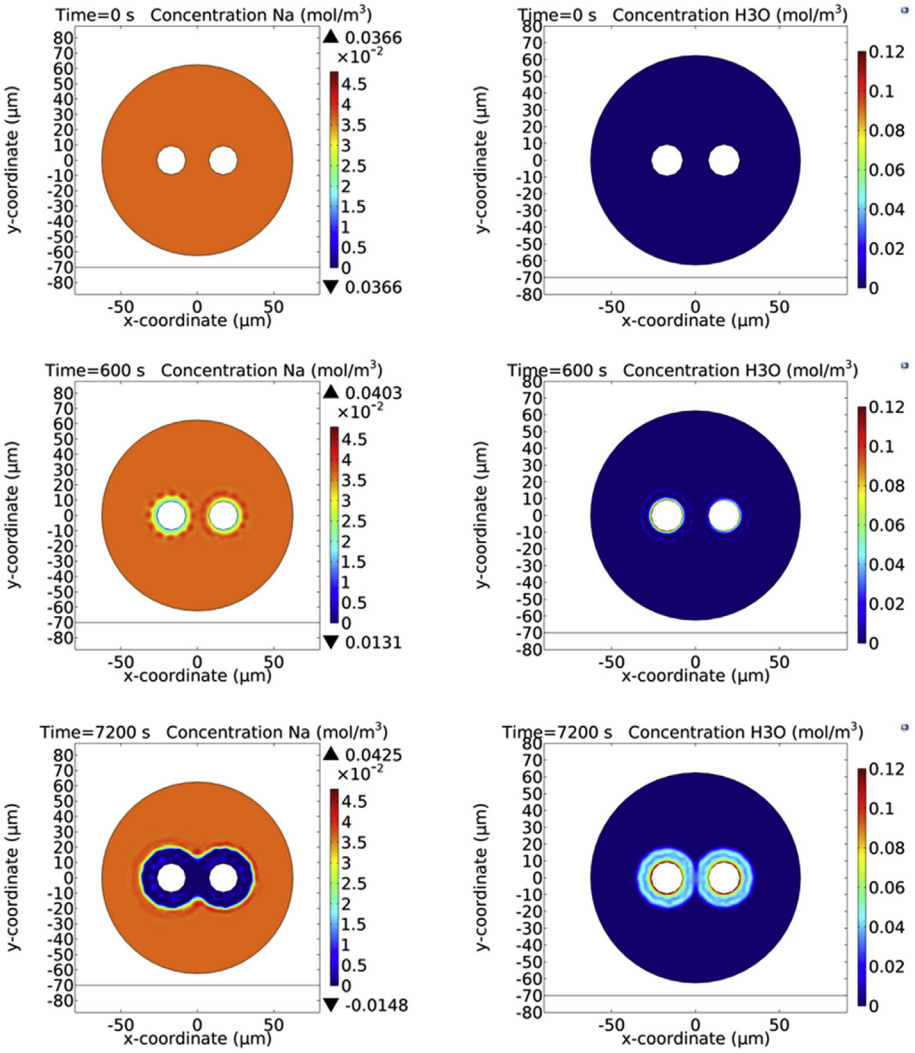

Fig. 10. Temporal evolution of the mobile positive ions obtained via the *far model* for induction poling. The electric potentials applied to the two floating electrodes assume the values (variable in time) calculated by means of the *near model* in the situation where the ground-plane is located 1 mm below the two adjacent fibers. The initial concentration of the impurity charges (Na^+) is assumed to be 1 ppm. The temperature of the sample in the simulation is assumed to be 300 °C while the injection of the hydrogenated species H_3O^+ is assumed to be inexhaustible and capable of neutralizing the *NBO* centres depleted of impurity positive ions due to the application of an external electric field.

5. Embedded electrodes for thermal poling of optical fibers

An important aspect which presents a limiting factor of the reliability of poled fibers as a potential technological platform for the realization of all-fiber nonlinear photonic devices is the incorporation of the electrodes themselves inside the cladding channels of the fiber. Few different solutions have been explored to overcome the limits of this technological aspect of thermal poling.

5.1. Solid electrodes

In section 3.2.3 we already briefly discussed problems associated with the manual insertion of solid electrodes, usually tungsten wires of diameters small enough to fit the cladding channels of a twin-hole silica fibers. This challenging and tedious manual process does not permit the insertion of wires longer than few centimetres. Moreover, the fact that the wire does not fit perfectly the hole but instead remains loose, causes a shape of the depletion region not geometrically regular, affecting the homogeneity of the effective nonlinearity created along the whole sample. From this point of view the development of the *induction poling* technique, allowing for poling an optical fiber without the need of a physical contact between the high voltage power supply and the embedded electrodes, represents a step forward towards the implementation of a more integrated platform for fabrication of all-fiber devices. Nevertheless, there are still some issues which the *induction poling* technique on its own does not solve completely. For example, the choice of filling the cladding holes with BiSn, as in Ref. [44], requires inserting the whole setup, including the pressurization system and the fiber to be filled, into an oven. Apart from this issue, some measurements realized during a first explorative phase of our work demonstrated that the presence of metal inside the cladding holes affects heavily the transmission losses of such a device (3–5 dB/cm at a pump wavelength of 1550 nm). Self-evidently these very large losses are very detrimental, in particular with the final aim of realizing an efficient nonlinear device, such as for example a frequency doubler. The need of removing easily the electrodes after poling becomes fundamental and this presents another issue, namely the removal of a solidified metal, such as the BiSn at room temperature.

5.2. Liquid electrodes

Given the challenge presented by the removal of metallic alloys with melting temperature higher than room temperature (such as for example BiSn), in 2017 De Lucia et al. explored the possibility of using conductive materials liquid at room temperature, with the final aim of simplifying the procedure of their removal. Two types of solutions have been conceived and tested, namely metallic and non-metallic liquid conductors [46]. If the liquid conductor is a metal, it is possible to describe the mechanism of electrical conduction in the same terms of the solid metal, that is in terms of valence electrons which are basically free to move under the effect of the application of an electric field. If the liquid conductor is non-metallic, but for example is an electrolytic

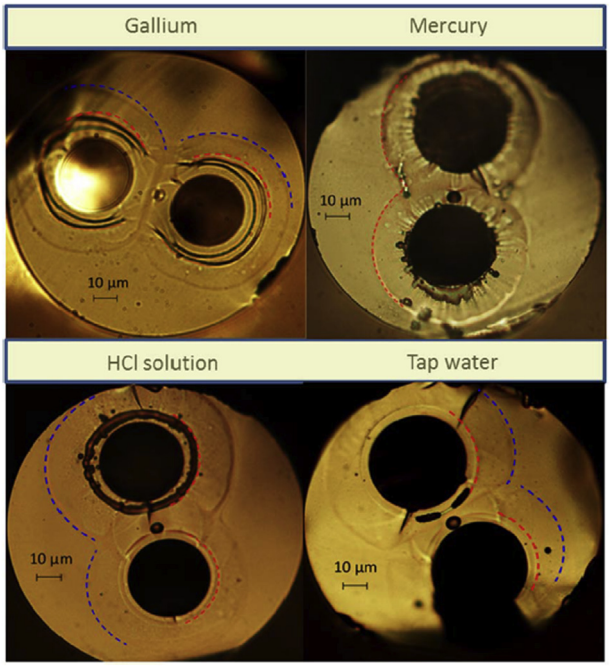

Fig. 11. Cross-sectional micrographs of the HF etched samples poled using novel liquid electrode types. The HF decorative etching process reveals the presence of depletion regions in all four twin-hole Ge-doped core, fused silica fibers. The observed dual concentric depletion region formation (highlighted by means of the red and blue dotted lines as a guide for the eye) is likely to be due to the Na and Li impurity charges involved in the electromigration process, typically characterized by differing ion mobilities in the glass [46]. (For interpretation of the references to colour in this figure legend, the reader is referred to the Web version of this article.)

solution (a liquid containing positive and negative mobile ions), electricity is conducted via the migration of positive and negative ions through the liquid. So, if a channel of the twin-hole fiber is filled with an electrolytic solution and a tungsten wire immersed into the solution in one end of the fiber and contacted to the anode of a high voltage power supply, the negative ions present in the solution would be attracted by the anode and positive ions would be repelled. The final result would be a liquid whose electric potential depends on the initial concentration of the free ions of the electrolytic solution. Indeed, the electrical conductivity of a non-metallic liquid depends upon the number of ions per unit volume and upon their drift velocity. Pure solvents such as water or alcohol are relatively poor electrical conductors, with an electrical conductivity of about $10^{-4}\ S/m$ [47]. The electrical conductivity of solutions of chemical salts in water is much higher, being about 10 S/m. Such solutions are generally classified as good conductors and are called electrolytic solutions. The dissolved substance, or solute, is known as the electrolyte. While the electrical conductivity of electrolytic solutions is quite high compared to the electrical conductivity of the pure solvent, their electrical conductivity is still small compared to a metallic conductor such as copper whose electrical conductivity at room temperature is about $0.6 \times 10^8\ S/m$, tungsten ($\approx 1.8 \times 10^7\ S/m$) or *BiSn* ($\approx 2.6 \times 10^6\ S/m$).

5.2.1. Metallic liquids

In Ref. [46] two different metallic liquids have been tested as embedded electrodes for thermal poling experiments, namely gallium and mercury.

Gallium is a metal characterized by some peculiar properties [48–50]. Some of these features include its very long liquid range, which goes from a supercooled state at 150 K to its boiling temperature of 2510 K, characterized by a low vapour pressure even at high temperatures, and an anomalous behaviour of its density upon its melting, which increases 3.2% while most metals decrease about 2–6% [51]. The melting temperature of solid gallium is 29.76 °C and its electrical conductivity is $\approx 3.7 \times 10^6\ S/m$, so it can be considered a very good electrical conductor. The most interesting feature of gallium is the structure of its liquid state. While most liquid metals can be considered as monoatomic simple liquids, this picture is not complete enough to describe the odd behaviour of gallium. One of the first intuitions on the structure of gallium is due to Ascarelli, who, in 1966, proposed a close similarity between the structure of liquid gallium and the one of the metastable $\beta - Ga$, which is the phase formed when the liquid is supercooled [52]. According to Ascarelli, $\beta - Ga$ could be considered the closest solid counterpart of liquid gallium, closer than $\alpha - Ga$, the solid gallium. A number of structural models have been proposed to explain the liquid state of gallium, and most of them agree in the assumption that in its liquid state, gallium presents two different coexisting structures, namely a layer lattice structure (which represents a reminder of the solid $\alpha - Ga$ and whose contribution is small) and a spherical close packing in the form of a straight atomic chain (typical of a simple liquid) [53]. This metastable nature of gallium makes the process of filling the cladding channels of a twin hole fiber somewhat unreliable. Gallium randomly goes from liquid to solid during the procedure of insertion of the electrodes and very often the formation of air gaps is observed, which compromises the electrical continuity of the embedded electrodes. Furthermore, even when its removal is feasible, because of its high viscosity, the amount of residues left inside the cladding channels after its removal process is high, affecting negatively the transmission losses of the all-fiber device. This and other issues motivated the exploration of other metals, in particular mercury.

Mercury is a chemical element with symbol Hg and atomic number 80. It is commonly known as *quicksilver* and is the only metallic element liquid at standard temperature and pressure (STP) conditions. Its melting and boiling temperatures are − 39 °C and 357 °C respectively. It is characterized by a very high density ($\approx 13.5 \times 10^3 Kg/m^3$ near room temperature) and an electrical conductivity of $\approx 1.4 \times 10^6\ S/m$. This value of conductivity makes mercury a very good conductor [54] and a reasonable replacement of gallium for creating liquid electrodes embedded into the channels of an optical fiber.

5.2.2. Non-metallic liquids

Although mercury represents a very efficient method for the

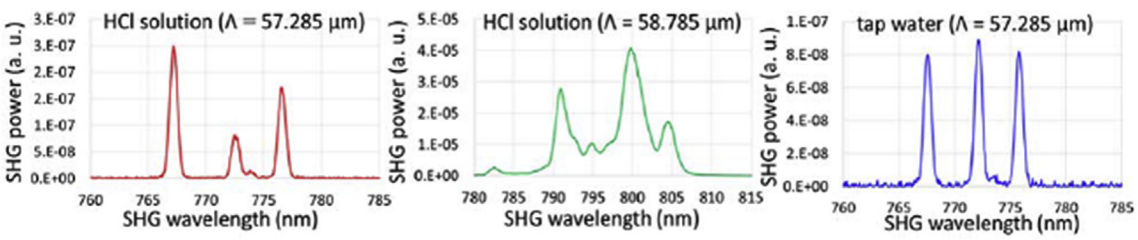

Fig. 12. SHG output spectra of optical fibers poled using a HCl solution, as well as ordinary tap water. Insertion loss at 1550 nm is 0.7 dB for water and 0.5 dB for HCl solution. The induced quadratic nonlinearity for both aqueous solutions is estimated at ≤ 0.001 p.m./V, assuming a fabricated device length of 20 cm and a modal overlap area of 49.43 μm^2 at 1550 nm pump wavelength.

creation of liquid electrodes for thermal poling of metre-long fibers because it can be easily introduced and removed afterwards from the channels of the fiber, it is undeniable that there is a relevant safety issue related to its usage. It is well known indeed that mercury is highly toxic, particularly for inhalation of its vapours [55]. Taking into account that mercury, used as electrode for thermal poling, is heated up to 300 °C a temperature very close to its boiling temperature (357 °C) it is obvious that during thermal poling some vapours of mercury could be created. Although the thermal poling experiments are realized inside a fume hood, this circumstance still represents a hazard which should be avoided. Furthermore, even during the filling process of the channels, realized at room temperature, there is a risk of evaporation, even if the amount of mercury manipulated during these phases of the work is very tiny. Another issue related to the use of mercury as embedded electrode is that, after its removal process, it leaves its traces on the inner surfaces of the fiber cladding channels. These traces are definitely less significant than gallium ones, but they are not negligible. For all these reasons it was later chosen to explore some electrolytic solutions as liquid electrodes for thermal poling experiments.

An ***electrolytic solution*** is a water-based solution containing a certain amount of ions (electrolytes), which could be charged up to a certain electrical potential if contacted to a voltage power supply [47]. A simple way to create an electrolytic solution is to dissolve a salt (solute) in water (solvent), producing a chemical reaction called solvation, which consists in a process of attraction and association of molecules of the solvent with molecules or ions of the solute. A salt is an ionic compound that results from the neutralization reaction of an acid and a base [56] and is composed of related numbers of cations (positively charged ions) and anions (negative ions) so that the product is electrically neutral (without a net charge). When they are dissolved in water, the ions they are made of separate and move independently through the solution as aqueous ions. Since ions are charged species their motion through space is equivalent to an electrical current. The property of conducting an electrical current makes the aqueous solution an electrolytic solution. An important advantage of using aqueous solutions instead of metallic liquids is that it is possible to fill (either selectively or otherwise) the channels of the optical fiber to be poled without the need of any pressurization system. The aqueous solution moves through the cylindrical channels of the fiber by capillary action.

5.3. Thermal poling of optical fibers with liquid electrodes

In the work of De Lucia et al. it is demonstrated for the first time the possibility of thermally poling optical fibers equipped with electrolytic solutions as embedded electrodes. In Fig. 11 a qualitative comparison between fibers poled with different electrodes is shown, which demonstrates the formation of a depletion region in all of them. The fibers were subsequently periodically erased to quasi-phase match the SHG between 1550 nm and 775 nm. Fig. 12 shows the second harmonic response, demonstrating the formation of an effective second order susceptibility even when aqueous solutions have been used.

5.3.1. Recent outcomes and conclusions

With respect to the state of art of thermal poling until five years ago, two important steps further have been realized towards the full exploitation of the thermal poling technique for poling optical fibers of arbitrary length and geometry. The use of liquid electrodes (both metallic and non-metallic), together with the *induction poling* technique, could allow for easily poling optical fibers of different geometry (conventional step-index, solid core microstructured, etc) and of different length. Among the most recent outcomes produced by the technological platform developed so far by De Lucia and co-workers there is the first demonstration of phase-matched parametric amplification via four-wave mixing (FWM) in an all-fiber setup including a high-power pulsed source, a periodically poled silica fiber (PPSF), and an optical microfiber (OMF). The PPSF generates a phase matched second harmonic (SH) signal and non-phase matched third harmonic (TH) signal via sum frequency generation (SFG), while inside the OMF a degenerate FWM process (involving two photons of the SH and one photon of FF and TH) is observed for two different diameters of the OMF [57]. A second work has been published where, adopting the PPSF in conjunction with two cascaded OMFs, all-fiberized fourth harmonic generation (FHG) and fifth harmonic generation (5HG) are achieved using the SH signal generated inside the PPSF and two cascaded FWM processes in the two OMFs [58]. In 2017 a last work related to high harmonics generation in PPSFs was published by Wang et al. where adopting the same all-fiber scheme of a PPSF followed by two cascaded OMFs, the SHG produced in the PPSF is in this case followed by third harmonic generation (THG) and FWM [59]. The most recent result concerns the first demonstration of a phase-sensitive amplification process in PPSF, realized by the group of Dr. Francois Leo, Université Libre de Bruxelles [60]. All these results clearly demonstrate that the road towards a full exploitation of thermal poling for fabrication of all-fiber nonlinear photonic devices, such as for example compact laser sources, quantum switches/modulators, sources of photon pairs for quantum optics, etc., has been just opened.

Declaration of interests

☒The authors declare that they have no known competing financial interests or personal relationships that could have appeared to influence the work reported in this paper.

☐The authors declare the following financial interests/personal relationships which may be considered as potential competing interests:

Author agreement declaration

The authors certify that we have both written, seen and approved the final version of the manuscript being submitted. As this is an invited review paper, by definition it contains original work that has been previously published elsewhere, but the review itself is not under consideration for publication anywhere else.

Funding

Engineering and Physical Sciences Research Council (EPSRC) (EP/I035307/1).

Data repositories can be found at the next links:

https://eprints.soton.ac.uk/386825/
https://eprints.soton.ac.uk/389375/
https://eprints.soton.ac.uk/387990/
https://eprints.soton.ac.uk/386031/
https://eprints.soton.ac.uk/386020/
https://eprints.soton.ac.uk/383708/

References

[1] J. Tyndall, On Some Phenomena Connected with the Motion of Liquids, Proc R Inst Great Britain, 1854, p. 446.
[2] J.L. Baird, An improved method of and means for producing optical images [Internet], British Patent No 285 (1928) 738. Available https://ci.nii.ac.jp/naid/10025347920/.
[3] C.W. Hansell, Picture Transmission [Internet], US Patent. 1751584 (1930) Available https://patentimages.storage.googleapis.com/07/66/87/78111772a09892/US1751584.pdf.
[4] F.P. Kapron, D.B. Keck, R.D. Maurer, Radiation losses in glass optical waveguides, Appl Phys Lett. American Institute of Physics 17 (1970) 423–425.
[5] P.N. Butcher, D. Cotter, The Elements of Nonlinear Optics, Vol. 9 of Cambridge Studies in Modern Optics, Cambridge University Press, Cambridge, UK, 1990.
[6] R.A. Myers, N. Mukherjee, S.R. Brueck, Large second-order nonlinearity in poled fused silica, Opt. Lett. 16 (1991) 1732–1734.
[7] R.G. Batchko, G.D. Miller, A. Alexandrovski, M.M. Fejer, R.L. Byer, Limitations of high-power visible wavelength periodically poled lithium niobate devices due to green-induced infrared absorption and thermal lensing, Technical Digest Summaries of Papers Presented at the Conference on Lasers and Electro-Optics Conference Edition 1998 Technical Digest Series, vol. 6, IEEE Cat No98CH36178, 1998, pp. 75–76.

[8] Y. Furukawa, K. Kitamura, A. Alexandrovski, R.K. Route, M.M. Fejer, G. Foulon, Green-induced infrared absorption in MgO doped LiNbO 3, Appl Phys Lett. AIP 78 (2001) 1970–1972.
[9] M. Yamane, Y. Asahara, Glasses for Photonics, Cambridge University Press, 2000.
[10] W.H. Zachariasen, The atomic arrangement in glass, J Am Chem Soc. American Chemical Society 54 (1932) 3841–3851.
[11] B.E. Warren, J. Biscob, Fourier analysis of x-ray patterns of soda-silica glass, J Am Ceram Soc. Wiley Online Library 21 (1938) 259–265.
[12] B.E. Warren, The basic principles involved in the glassy state, J Appl Phys. American Institute of Physics 13 (1942) 602–610.
[13] P.S. Paufler, R. Elliott, Physics of Amorphous Materials vol. 20, Longman Group Ltd., London, New York, 1984 Pp X + 386. Price: £ 25.00. ISBN 0–582–44636–8. Cryst Res Technol. 1985 1238–1238.
[14] B.E.A. Saleh, M.C. Teich, B.E. Saleh, Fundamentals of Photonics, Wiley, New York, 1991.
[15] Y. Fujii, B.S. Kawasaki, K.O. Hill, D.C. Johnson, Sum-frequency light generation in optical fibers, Opt. Lett. 5 (1980) 48.
[16] Y. Sasaki, Y. Ohmori, Phase-matched sum-frequency light generation in optical fibers, Appl Phys Lett. American Institute of Physics 39 (1981) 466–468.
[17] Y. Ohmori, Y. Sasaki, Two-wave sum-frequency light generation in optical fibers, IEEE J. Quantum Electron. 18 (1982) 758–762.
[18] J.-M. Gabriagues, L. Fersing, Second and third harmonic generation in optical fibers, Conference on Lasers and Electro-Optics, Optical Society of America, 1984, p. THI33.
[19] U. Osterberg, W. Margulis, Dye laser pumped by Nd:YAG laser pulses frequency doubled in a glass optical fiber, Opt. Lett. 11 (1986) 516–518.
[20] U. Osterberg, W. Margulis, Experimental studies on efficient frequency doubling in glass optical fibers, Opt. Lett. 12 (1987) 57–59.
[21] R.H. Stolen, H.W. Tom, Self-organized phase-matched harmonic generation in optical fibers, Opt. Lett. 12 (1987) 585–587.
[22] D.S. Bethune, Quadrupole second-harmonic generation for a focused beam of arbitrary transverse structure and polarization, Opt. Lett. 6 (1981) 287–289.
[23] M.C. Farries, J. S.T, P. Russell, M.E. Fermann, D.N. Payne, Second-harmonic generation in an optical fiber by self-written $\chi(2)$ grating, Electron Lett. IET Digital Library 23 (1987) 322–324.
[24] R.W. Terhune, D.A. Weinberger, Second-harmonic generation in fibers, J Opt Soc Am B, JOSAB 4 (1987) 661–674 Optical Society of America.
[25] D.M. Krol, D.J. Digiovanni, W. Pleibel, R.H. Stolen, Observation of resonant enhancement of photoinduced second-harmonic generation in Tm-doped aluminosilicate glass fibers, Opt. Lett. 18 (1993) 1220–1222.
[26] R. Kashyap, Phase-matched periodic electric-field-induced second-harmonic generation in optical fibers, J Opt Soc Am B, JOSAB 6 (1989) 313–328 Optical Society of America.
[27] N. Mukherjee, R.A. Myers, S.R.J. Brueck, Dynamics of second-harmonic generation in fused silica, J Opt Soc Am B, JOSAB 11 (1994) 665–669 Optical Society of America.
[28] T.G. Alley, S.R.J. Brueck, R.A. Myers, Space charge dynamics in thermally poled fused silica, J. Non-Cryst. Solids 242 (1998) 165–176.
[29] K. Yamamoto, H. Namikawa, The irreversible and reversible changes in silica glasses observed by electrical properties (Part 1), J Ceram Soc Jpn. The Ceramic Society of Japan 102 (1994) 658–664.
[30] K. Yamamoto, H. Namikawa, The irreversible and reversible changes in silica glasses observed by electrical properties (Part 2), J Ceram Soc Jpn. The Ceramic Society of Japan 103 (1995) 910–916.
[31] A. Kudlinski, Y. Quiquempois, G. Martinelli, Modeling of the chi(2) susceptibility time-evolution in thermally poled fused silica, Optic Express 13 (2005) 8015–8024.
[32] A. Kudlinski, Y. Quiquempois, M. Lelek, H. Zeghlache, G. Martinelli, Complete characterization of the nonlinear spatial distribution induced in poled silica glass with a submicron resolution, Appl Phys Lett. American Institute of Physics 83 (2003) 3623–3625.
[33] P.G. Kazansky, L. Dong, P.S. Russell, High second-order nonlinearities in poled silicate fibers, Opt. Lett. 19 (1994) 701–703.
[34] T. Fujiwara, D. Wong, S. Fleming, Large electrooptic modulation in a thermally-poled germanosilicate fiber, IEEE Photonics Technol. Lett. 7 (1995) 1177–1179.
[35] P.G. Kazansky, V. Pruneri, Electric-field poling of quasi-phase-matched optical fibers, J Opt Soc Am B, JOSAB 14 (1997) 3170–3179 Optical Society of America.
[36] D. Wong, W. Xu, S. Fleming, M. Janos, K.-M. Lo, Frozen-in electrical field in thermally poled fibers, Opt. Fiber Technol. 5 (1999) 235–241.
[37] P. Blazkiewicz, W. Xu, D. Wong, S. Fleming, T. Ryan, Modification of thermal poling evolution using novel twin-hole fibers, J. Light. Technol. 19 (2001) 1149–1154.
[38] P. Blazkiewicz, W. Xu, D. Wong, S. Fleming, Mechanism for thermal poling in twin-hole silicate fibers, J Opt Soc Am B, JOSAB. Optical Society of America 19 (2002) 870–874.
[39] N. Myrén, H. Olsson, L. Norin, N. Sjödin, P. Helander, J. Svennebrink, et al., Wide wedge-shaped depletion region in thermally poled fiber with alloy electrodes, Optic Express 12 (2004) 6093–6099.
[40] T.G. Alley, S.R. Brueck, Visualization of the nonlinear optical space-charge region of bulk thermally poled fused-silica glass, Opt. Lett. 23 (1998) 1170–1172.
[41] W. Margulis, O. Tarasenko, N. Myrén, Who needs a cathode? Creating a second-order nonlinearity by charging glass fiber with two anodes, Optic Express 17 (2009) 15534–15540.
[42] A. Camara, O. Tarasenko, W. Margulis, Study of thermally poled fibers with a two-dimensional model, Optic Express 22 (2014) 17700–17715.
[43] H. Knape, W. Margulis, All-fiber polarization switch, Opt. Lett. 32 (2007) 614–616.
[44] F. De Lucia, D. Huang, C. Corbari, N. Healy, P.J.A. Sazio, Optical fiber poling by induction, Opt. Lett. 39 (2014) 6513–6516.
[45] F. De Lucia, D. Huang, C. Corbari, N. Healy, P.J.A. Sazio, Optical fiber poling by induction: analysis by 2D numerical modeling, Opt. Lett. 41 (2016) 1700–1703.
[46] F. De Lucia, D.W. Keefer, C. Corbari, P.J.A. Sazio, Thermal poling of silica optical fibers using liquid electrodes, Opt. Lett. 42 (2017) 69–72.
[47] H. Semat, R. Katz, Electrical Conduction in Liquids and Solids. Physics vol. 28, Rinehart & Company Inc, New York, USA, 1958, pp. 524–538.
[48] T.W. Richards, S. Boyer, FURTHER STUDIES CONCERNING GALLIUM. Its electrolytic behavior, purification, melting point, density, coefficient of expansion, compressibility, surface tension, and latent heat of fusion, J Am Chem Soc. American Chemical Society 43 (1921) 274–294.
[49] R.N. Lyon, Liquid-Metals Handbook, US Government Printing Office, Washington. D C June, 1952.
[50] A. Defrain, Metastable states of Ga–Supercooling and polymorphism, J Chim Phys 74 (1977) 851–862.
[51] H.Y. Park, M.S. Jhon, Thermodynamic and Transport Properties of Liquid Gallium. Nuclear Engineering and Technology, dbpia.co.kr, 1982 Available http://www.dbpia.co.kr/Journal/ArticleDetail/NODE02252216.
[52] P. Ascarelli, Atomic radial distributions and ion-ion potential in liquid gallium, Phys Rev. American Physical Society 143 (1966) 36–47.
[53] H. Richter, Solid amorphous Bi, Ga, and Fe as examples of liquid-like amorphous substances, J Vac Sci Technol B Nanotechnol Microelectron. American Vacuum Society 6 (1969) 855–858.
[54] D.W.H. Rankin, CRC handbook of chemistry and physics, in: David R. Lide (Ed.), Crystallography Rev, 89th edition, vol. 15, Taylor & Francis, 2009, pp. 223–224.
[55] M. Shepherd, S. Schuhmann, R.H. Flinn, J.W. Hough, P.A. Neal, Hazard of mercury vapor in scientific laboratories, J. Res. Natl. Bur. Stand. 26 (1941) 9.
[56] T.J. Wenzel, Douglas A. Skoog, Donald M. West, F. James Holler, Stanley R. Crouch, Fundamentals of Analytical Chemistry, 9th ed., International, vol. 405, 2013, pp. 7903–7904. Anal Bioanal Chem.
[57] M.I.M. Abdul Khudus, F. De Lucia, C. Corbari, T. Lee, P. Horak, P. Sazio, et al., Phase matched parametric amplification via four-wave mixing in optical microfibers, Opt. Lett. 41 (2016) 761–764.
[58] M.I.M.A. Khudus, M.I. Abdul, T. Lee, F. De Lucia, C. Corbari, P. Sazio, et al., All-fiber Fourth and Fifth Harmonic Generation from a Single Source [Internet], Optics Express, 2016, p. 21777, https://doi.org/10.1364/oe.24.021777.
[59] Wang, et al., Y, All-fiber sixth-harmonic generation of deep UV, Opt. Lett. 42 (2017) 4671–4674.
[60] N. Englebert, F. De Lucia, P.J.A. Sazio, S.-P. Gorza, F. Leo, Phase Sensitive Amplification in a Periodically Poled Fiber, Cleo Europe, 2019 (accepted).